

CCNA2 and NEK2 regulate glioblastoma progression by targeting the cell cycle

HAO-YU ZHOU*, YI-CHANG WANG*, TUO WANG, WEI WU, YI-YANG CAO,
BEI-CHEN ZHANG, MAO-DE WANG and PING MAO

Department of Neurosurgery, The First Affiliated Hospital of Xi'an Jiaotong University, Xi'an, Shaanxi 710061, P.R. China

Received September 19, 2023; Accepted February 5, 2024

DOI: 10.3892/ol.2024.14339

Abstract. Glioblastoma (GBM) is characterized by significant heterogeneity, leading to poor survival outcomes for patients, despite the implementation of comprehensive treatment strategies. The roles of cyclin A2 (CCNA2) and NIMA related kinase 2 (NEK2) have been extensively studied in numerous cancers, but their specific functions in GBM remain to be elucidated. The present study aimed to investigate the potential molecular mechanisms of CCNA2 and NEK2 in GBM. CCNA2 and NEK2 expression and prognosis in glioma were evaluated by bioinformatics methods. In addition, the distribution of CCNA2 and NEK2 expression in GBM subsets was determined using pseudo-time analysis and tricycle position of single-cell sequencing. Gene Expression Omnibus and Kyoto Encyclopedia of Genes and Genome databases were employed and enrichment analyses were conducted to investigate potential signaling pathways in GBM subsets and a nomogram was established to predict 1-, 2- and 3-year overall survival probability in GBM. CCNA2 and NEK2 expression levels were further validated by western blot analysis and immunohistochemical staining in GBM samples. High expression of CCNA2 and NEK2 in glioma indicates poor clinical outcomes. Single-cell sequencing of GBM revealed that these genes were upregulated in a subset of positive neural progenitor cells (P-NPCs), which showed significant proliferation and progression properties and may activate G2M checkpoint pathways. A comprehensive nomogram predicts 1-, 2- and 3-year overall survival probability in GBM by considering P-NPCs, age, chemotherapy and radiotherapy scores. CCNA2 and NEK2

regulate glioblastoma progression by targeting the cell cycle, thus indicating the potential of novel therapy directed to CCNA2 and NEK2 in GBM.

Introduction

Glioblastoma (GBM) is the most common type of malignant tumor in the central nervous system among adults and is associated with a poor survival rate (1). Despite significant advancements in surgical techniques, radiotherapy and chemotherapy, the prognosis for GBM remains dismal (2). The malignant behavior of cancer cells is regulated by oncogenes and tumor suppressor genes through various signaling pathways, which significantly affect the efficacy of clinical treatments and patient outcomes (3,4). The development of GBM requires specific molecular aberrations, including mutations in the P53 and retinoblastoma signaling pathways, as well as alterations in the receptor tyrosine kinase/Ras/phosphoinositide 3-kinase (PI3K)/protein kinase B (AKT) signaling pathways and the epithelial growth factor receptor (5,6). Despite efforts to target these abnormal changes, GBM treatment has not yielded favorable results. Hence, there is an urgent need to identify novel biomarkers and therapeutic targets in GBM.

A previous study revealed that NIMA related kinase 2 (NEK2) overexpression was significantly correlated with the grade, proliferation and prognosis of GBM (7). In addition, it enhances malignancy through the NIK/NF- κ B pathway (8). The NEK family is a group of protein kinases that share similarities with NIMA kinase, found in higher eukaryotes (9). This family comprises 11 members, designated as NEK 1 to 11, with NEK2 exhibiting the highest similarity to NIMA (9). NEK2 is primarily located in cell centrosomes and is involved in various cellular processes, including centrosomal circulation during cell mitosis, formation of bipolar mitotic spindles (10) and stabilization of microtubules (11). Abnormal overexpression of NEK2 has been observed in several types of human cancers, including non-small cell lung cancer (12), myeloma (13), pancreatic (14) and breast cancer (15). This overexpression has been associated with various aspects of malignant transformation, such as tumorigenesis, therapy resistance and tumor progression (16).

Cyclin A2 (CCNA2) is a gene related to the cell cycle that has been suggested as a possible molecular marker in low-grade gliomas (17). This gene is in the Q27 region of

Correspondence to: Dr Ping Mao or Dr Mao-De Wang, Department of Neurosurgery, The First Affiliated Hospital of Xi'an Jiaotong University, 277 West Yanta Road, Xi'an, Shaanxi 710061, P.R. China
E-mail: mp101010@sina.com
E-mail: maodewang@163.com

*Contributed equally

Key words: cyclin A2, NIMA-related kinase 2, glioblastoma, single cell sequencing, cell cycle

human chromosome 4 and plays a crucial role in promoting the transition through the G1/S and G2/M phases of the cell cycle by binding and interacting with cyclin-dependent kinases CDK1 and CDK2 (18). Furthermore, the complete absence of CCNA2 leads to embryonic lethality in mice (19). CCNA2 is differentially expressed in several types of tumors in the digestive, urinary and central nervous systems (20). It has been found to play a regulatory role in the development of kidney cancer (20), breast cancer (21), lung cancer (22), colorectal cancer (23) and other types of tumors. Moreover, CCNA2 has been demonstrated to regulate epithelial-mesenchymal transition in distinct types of cancer, including oral squamous cell carcinoma (24), colorectal cancer (25) and bladder cancer (26). CCNA2 and NEK2 have been also identified as crucial genes in cancer transformation induced by hepatitis B (27) and the progression and prognosis of pancreatic cancer (28). However, the specific roles and correlation of CCNA2 and NEK2 with GBM have not been yet elucidated.

In the present study, it was observed that high expression of CCNA2 and NEK2 in glioma indicates poor clinical outcomes. Furthermore, CCNA2 and NEK2 were significantly co-expressed in neural progenitor cells (NPCs) at the single-cell level. Moreover, CCNA2 and NEK2, along with NPCs, were closely linked to the cell cycle in GBM and controlled the malignant advancement of tumor cells. Based on these findings, a comprehensive nomogram that supports a clinical prognosis analysis has been developed, which may prompt the development of new treatment strategies.

Materials and methods

Data collection. A total of 693 expression profiles of bulk sequencing and relevant clinical data for glioma were extracted from the Chinese Glioma Genome Atlas (CGGA; <http://www.cgga.org.cn/>) (29) and The Cancer Genome Atlas Program (TCGA; <https://www.cancer.gov/ccg/research/genome-sequencing/tcga>) (30). The single cell RNA sequencing (scRNA-seq) expression profile and relevant clinical data of nine isocitrate dehydrogenase (IDH) wildtype GBM samples were collected from the Gene Expression Omnibus (GEO) database, with accession number GSE131928 (31). Data were obtained using 10X scRNA-seq.

Cellular clustering, gene analysis and cell type annotation of scRNA-seq. The gene expression matrix and corresponding clinical information for the nine IDH wildtype GBM samples were imported into RStudio (v.4.3.0; r-project.org) and analyzed using the Seurat package (v.4.0; [R; r-project.org](http://r-project.org)) (32). Downstream analysis was performed on the primary expression data, removing low-quality single cells. Cells with <300 expressed genes, >10% mitochondrial transcripts, >0.5% red blood cell transcripts, or genes that were expressed in fewer than three individual cells were also excluded. After excluding 2,841 low-quality cells, the expression data from the remaining 13,360 single cells were normalized using the 'LogNormalize' method. The top 5,000 highly variable features were then selected using the 'FindVariableFeatures' method, with variance stabilizing transformation. Next, the gene expression data were transformed using the z-score method and scaled by the 'ScaleData'. The linear method was used to scale and

center the top 5,000 highly variable features in this dataset, after which the principal component analysis was performed to reduce the dimensionality of the data. The top 5,000 most variable genes in the dataset were used for this analysis. The first 20 principal components (PCs) were analyzed using the 'JackStrawPlot' and 'ElbowPlot'. These 20 PCs were then used for downstream calculations based on 'FindNeighbors' with default parameters. The resolution parameter applied to identify clusters by 'FindClusters' was 0.5, which was determined based on the range of 0.1 to 1 for the single-cell datasets. The t-distributed stochastic neighbor embedding (t-SNE) was employed to perform non-linear dimensionality reduction and visualize different single-cell clusters. Marker genes for each cluster were identified using 'FindAllMarkers'. Only the top five significantly upregulated genes were selected for presentation in the heatmap, based on the following criteria: Adjusted P-value <0.05, minimal percentage >0.25 and log₂-fold change (log₂FC) >0.25. Subsequently, SingleR (Bioconductor-SingleR) and Cellmarker 2.0 (<http://bio-bigdata.hrbmu.edu.cn/CellMarker/index.html>) were used together to annotate cell types for the different single-cell clusters (33,34).

Evaluation of stemness in single-cell clusters using scRNA-seq. Cellular trajectory reconstruction analysis using gene counts and expression (CytoTRACE) is an emerging computational method for evaluating the transcriptional diversity of each single-cell cluster in terms of differential or stemness status based on scRNA-seq. This method has been validated in large-scale datasets and has exceeded pre-existing computational strategies for evaluating stemness (35). The CytoTRACE package (v.0.3.3; CytoTRACE) was used to calculate the CytoTRACE score for each single-cell cluster. This score ranges from 0 to 1, with a higher score indicating greater stemness or fewer differentiation characteristics.

Pseudo-time trajectory analysis of scRNA-seq. The Monocle 2 package (v.2.28.0; Monocle; cole-trapnell-lab.github.io) was utilized to perform trajectory analysis, assuming that the one-dimensional variable 'time' captures the high-dimensional expression characteristics and reveals the transformation of cell status based on scRNA-seq data (36). The cell types identified as astrocytes and NPC clusters were further analyzed for trajectory features, using Monocle 2. The 'newCellDataSet' function was applied to establish an analysis purpose with the parameter 'expressionFamily=negbinomial.size'. Subsequently, the highly variable genes generated from the 'VariableFeatures' were utilized to reduce dimensions and sort cells in pseudo-time, using the 'reduceDimension' function with the 'DDRTree' algorithm. To identify candidate genes that separate cells into branches, a filtering criterion of 'mean expression ≥0.5' and 'dispersion empirical ≥1x dispersion_fit' was used. The branch expression analysis modeling (BEAM) was employed to analyze expression data and identify significant genes with a Q-value <0.0001. These genes were then grouped into different subgroups based on their expression patterns.

Estimating the cell cycle phase of scRNA-seq data. The tricycle package (v.1.8.0; bioconductor.org) was used to evaluate cell cycle phases by leveraging critical characteristics of

cell cycle biology. This method has been positively compared with gold-standard experimental assays and has demonstrated significant predictive potential with multiple cell types or tissues in single-cell datasets (37). The preprocessed scRNA-seq dataset was evaluated for cell cycle phase, using the default parameters of the tricycle package. This package calculated a cell cycle position, represented by polar coordinates ranging from 0 to 2π , indicating distinct phases.

Estimating the proportion of positive NPCs (P-NPCs) in bulk sequencing samples. P-NPCs were defined as NPCs with CCNA2 and NEK2 expression levels >0 . The marker genes were identified using 'FindMarkers', with a threshold of $\log_2FC >1$, an adjusted P-value <0.05 and a minimum percentage >0.70 . The proportion of P-NPCs in bulk sequencing samples was evaluated through single-sample gene set enrichment analysis (ssGSEA), using marker genes.

Analysis of differentially expressed genes (DEGs) in bulk sequencing. Preprocessing of the expression profile from bulk sequencing included background correction, gene symbol transformation and normalization using RStudio programming. Significant DEGs in these datasets were found using the limma package (version 3.48.3; Bioconductor). Genes were considered as upregulation with adjusted P-value <0.05 and \log_2 -fold change (\log_2FC) >1.5 and the downregulated genes had an adjusted P-value of <0.05 and a \log_2 -fold change (\log_2FC) <-1.5 .

Gene ontology (GO), Kyoto Encyclopedia of Genes and Genomes (KEGG), gene set enrichment analysis (GSEA) and gene set variation analysis (GSVA). Candidate genes resulting from bulk sequencing analysis or scRNA-seq analysis were used to conduct GO and KEGG analyses, using the clusterProfiler package (v.4.8.1; Bioconductor). Gene sets were evaluated according to the hallmark gene sets in the MSigDB database (gsea-msigdb.org/gsea/msigdb/index.jsp) (38). The results met the requirements, with an adjusted P-value of <0.05 (39). Furthermore, the GSEA was utilized to identify enriched pathways from the previous analyses of bulk sequencing or scRNA-seq. The significantly enriched results were subsequently validated using GSVA.

Establishing and assessing the predictive nomogram. To construct a nomogram that predicts the prognosis of patients with GBM, a multivariate Cox regression analysis to identify significant independent risk and protective factors was conducted. Based on these factors, a comprehensive nomogram was developed. The predictive potential of the nomogram was also demonstrated by the calibration curve. The suitability of the current predictors used in the nomogram was tested by evaluating the Schoenfeld residuals and deviance residuals to assess the proportional hazards assumption and identify outliers. Decision curve analysis (DCA) was also performed to assess the clinical applicability of the nomogram and the net benefit of diverse prediction models at different threshold probabilities. This was achieved by adding the benefits and minimizing the harms. The time-dependent receiver operating characteristic (ROC) curve was used to detect the discrimination of the nomogram and the Kaplan-Meier curve was used to estimate the prognostic value of the nomogram score.

Acquisition of glioma tissue. A total of 18 samples included World Health Organisation (WHO) II, III and IV grade gliomas were obtained from patient samples with a pathological diagnosis, who underwent craniotomy at the First Affiliated Hospital of Xi'an Jiao Tong University from April 2022 to December 2022. Of 18 patients, 8 were female and 10 were male. The mean age was 56 years (range, 42-69 years). The grades of the 18 glioma samples were confirmed by two independent pathologists. Inclusion criteria: i) Glioma patients meeting the 5th edition of the World Health Organization classification of tumors of the central nervous system in 2021; ii) All patients received conventional imaging examination within 1 week before surgery and were diagnosed with glioma; iii) the first diagnosed case without any invasive or non-invasive treatment; iv) Age above 18 years old, regardless of gender; v) The tumor was supratentorial. Exclusion criteria: i) Patients with other types of brain tumors; ii) patients who could not receive surgical treatment due to physical, financial or other reasons. The research involving the utilization of these biological specimens received ethical approval from the Ethics Committee of the hospital located in Xi'an, Shaanxi, China (approval no. 2020-G13). Informed consents for the utilization of clinical samples were approved and signed by patients.

Immunohistochemistry staining. For the immunohistochemical study, tissue blocks were fixed in 4% paraformaldehyde (PFA) at 4°C for 48 h, embedded in paraffin and sectioned at a thickness of 4 μ m. The processed sections were blocked with 5% bovine serum albumin (BSA, EZ2811C238; BioFroxx) for 1 h at room temperature. Then the tissue sections were incubated with primary antibodies (1:100) to NEK2 and CCNA2 overnight at 4°C, after which they were incubated with biotinylated secondary antibodies (1:2,000) at room temperature for 1 h. Next, sections were incubated with horseradish peroxidase-conjugated avidin (PK4002; NEOBIOSCIENCE) at room temperature for 1 h, washed with PBS and stained with 3,3'-diaminobenzidine (30 mg dissolved in 100 ml of Tris buffer containing 0.03% H_2O_2) at room temperature for 5 min. The sections were then rinsed in water and counterstained with hematoxylin at room temperature for 3 min. For the evaluation of NEK2 and CCNA2 expression, 10 visual fields per section were randomly selected and examined by light microscopy. The present study utilized the following antibodies: Mouse anti-NEK2 primary antibodies (1:100, sc-55601; Santa Cruz Biotechnology, Inc.) and rabbit anti-CCNA2 primary antibodies (1:100, ab181591; Abcam). Goat anti-rabbit IgG (1:2,000, ab97051; Abcam) and Goat anti-mouse IgG (1:2,000, PK4002; NEOBIOSCIENCE) was used as the secondary antibody. The results were analyzed using the ImageJ (v.1.8.0) software (National Institutes of Health).

Western blot analysis. The samples were prepared in RIPA buffer; Servicebio Biological) containing a protease inhibitor cocktail (MilliporeSigma) were used for western blot analysis. And the protein concentration was measured using a BCA protein assay kit (Beyotime Biotechnology). Equal amounts of protein lysates were loaded onto the wells (20 μ g/lane) of a 10% precast SDS-PAGE gel and transferred to a PVDF membrane (Thermo Fisher Scientific, Inc.; Invitrogen). The membrane was then incubated with 5% skimmed milk for 1 h at 25°C,

followed by overnight treatment with the target antibodies (anti-NEK2, 1:500; anti-CCNA2 primary antibody, 1:1,000) at 4°C. Following three washes with TBS-Tween 20 (TBST; 0.1% Tween) for 10 min each, the membrane was incubated with horseradish peroxidase-conjugated secondary antibodies (1:5,000) for 1 h at room temperature. The Amersham ECL Western Blot System (Cytiva) was applied to visualize the protein expression levels of each sample, using GAPDH (1:5,000) as the loading control. The following antibodies were used: Mouse anti-NEK2 primary antibody, rabbit anti-CCNA2 primary antibody, mouse GAPDH antibody (1:5,000, sc-47724; Santa Cruz Biotechnology, Inc.), Goat Anti-Mouse secondary antibody (1:5,000, DY60203; DIYIBio) and mouse anti-rabbit secondary antibody (1:5,000, sc-2357; Santa Cruz Biotechnology). Western blot analysis results were analyzed using the ImageJ (v.1.8.0) software.

Statistical analysis. Statistical analyses were performed using RStudio. Data were presented as the mean \pm standard deviation of triplicate determinations. The normality of the data distribution was evaluated by the Shapiro-Wilk test. Unpaired two-tailed Student's t-tests were performed to evaluate statistical differences in two groups and one-way ANOVA analyses following Tukey's multiple comparisons test was applied for comparisons between multiple groups and other statistical analysis methods were consistent with R packages listed in the manuscript. The log-rank test was utilized to conduct the Kaplan-Meier survival analysis. Multivariate Cox stepwise regression was selected for further analysis of survival. The P-value <0.05 indicated statistically significant differences.

Results

Highly expression of CCNA2 and NEK2 in glioma. The TCGA and CGGA databases were utilized to investigate the functions of CCNA2 and NEK2 in glioma. Results indicated a significant increase in the expression levels of CCNA2 and NEK2 with the progression of WHO grade in GBM (Fig. 1A, B, D and E). A significant positive correlation between the expression of CCNA2 and NEK2 in GBM was also observed (Fig. 1C and F). The Kaplan-Meier survival analysis revealed that patients with high expression of CCNA2 and NEK2 had a shorter overall survival time in GBM and all grades (Fig. 1G-K). To investigate the consistency of CCNA2 and NEK2 expression levels in clinical glioma samples, IHC staining was performed on glioma samples. Results indicated that CCNA2 and NEK2 gene expression levels significantly increased with the progression of WHO grade in glioma (Fig. 1L). The western blot analysis of clinical samples yielded comparable results (Fig. 1M). Original figures of western blot were presented in Fig. S1.

CCNA2 and NEK2 are co-expressed in NPC subtypes. Although a consistent expression of CCNA2 and NEK2 was demonstrated, the heterogeneity of GBM contributed to ambiguity regarding the reciprocal regulation within the same cells (40). Therefore, the expression pattern of CCNA2 and NEK2 was explored using scRNA-seq information collected from the GEO database (dataset no. GSE131928) to identify whether they were expressed in the same cell types. After

conducting quality control, low-quality cells were eliminated and 13,360 cells were retained for further analysis (Fig. S2). Cells from nine patients were clustered into 16 distinct groups, using t-SNE dimensionality reduction (Fig. 2A). To differentiate between cell types in the GBM microenvironment, immune and non-immune clusters were classified based on marker genes identified in previous studies (41-58). Genes such as CIQB (41), CD68 (42), CSF1R (43), PTPRC (44), CIQC (45), P2RY12 (46), CX3CR1 (47), CD163 (48), PTGS2 (49) and CD86 (50) were used to identify immune clusters; whereas genes AQP4 (51), PTPRZ1 (52), CLDN5 (53), CD34 (54), GFAP (55), FDGFRA (56), OLIG2 (57) and PLP1 (58) were used to identify non-immune clusters. Clusters 0, 2, 6, 14 and 15 were identified as immune cells, whereas clusters 1, 3, 4, 5, 7, 8, 9, 10, 11, 12 and 13 were identified as non-immune cells based on the average expression of PTPRC, as demonstrated in Fig. 2B and C. The top five significantly DEGs (marker genes) among these 16 clusters are presented in Fig. 2D. Based on the information provided by the singleR and CellMarker databases, nine distinct cell types out of the 16 clusters that were identified through the use of 'FindAllMarkers' were accurately annotated (Fig. 2E). According to Neftel *et al.* (31), the following cell types were considered malignant: Astrocytes, cancer stem cells, mesenchymal, NPCs, oligodendrocytic precursor cells and radial glia. Notably, the results showed significant heterogeneity in the proportions of various cell types present among different patients (Fig. 2F). Consequently, gene expression levels were analyzed in various cell types, revealing that CCNA2 and NEK2 were expressed in NPCs, belonging to cluster 11, which were derived from patient 'MGH143' (Fig. 2G-I). Although clusters 3, 11 and 13 were defined as NPCs, only cluster 11 expressed CCNA2 and NEK2, indicating that different subtypes of NPCs may possess distinct functions. CCNA2 is a ubiquitously expressed member of the cyclin family (59,60), it is commonly associated with cell proliferation and it is expressed at high levels in many cancers (61). NEK2 is a core component of the human centrosome (62), where it regulates a key step in the centrosome cycle, namely centrosome disjunction (63), which has been associated with the progression of a variety of cancers (64). Therefore, it was hypothesized that cluster 11, which co-expressed CCNA2 and NEK2, has the potential to stimulate cell proliferation and differentiation.

NPCs exhibit significant stemness in GBM. As aforementioned, it was revealed that cluster 11, which exhibited high expression of CCNA2 and NEK2, was upregulated in the 'MGH143' patient. GBM cells obtained from this patient were then divided into 10 clusters, using t-SNE dimensionality reduction (Fig. 3A). Marker genes were identified as the top three differential genes in each cluster (Fig. 3B). According to the SingleR and CellMarker databases, four cell types including NPC, astrocytes, neurons and tumor-associated macrophages (TAMs) were annotated. Clusters 3 and 4 were identified as NPCs (Fig. 3C). Since NPCs may function as the initiating cells of GBM (65,66), these four cell types were evaluated using the CytoTRACE package. The results demonstrated that NPCs had a higher potential to proliferate and differentiate (Fig. 3D and E). Moreover, when projected into these four cell types, CCNA2 and NEK2 were co-expressed in cluster 3 (Fig. 3F-H).

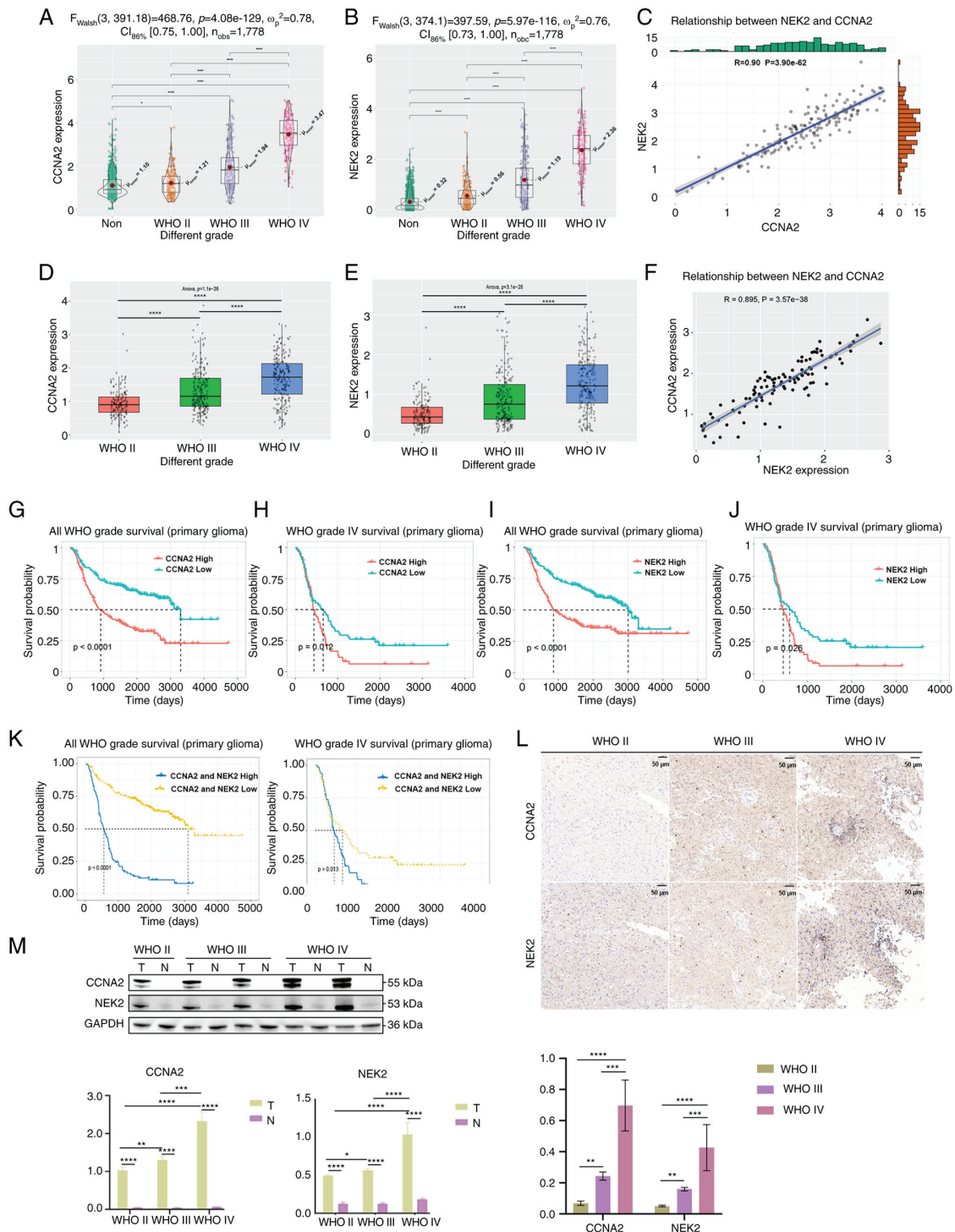


Figure 1. Highly expressed CCNA2 and NEK2 in glioma. (A) Analysis of NEK2 expression in different WHO grades of glioma, using TCGA database ($P < 0.05$ and $****P < 0.0001$, with independent t-test). (B) Analysis of NEK2 expression in different WHO grades of glioma, using TCGA database. (C) Co-expression analysis of CCNA2 and NEK2 expression in GBM, using TCGA database ($P < 0.0001$, with Pearson correlation coefficient). (D) Analysis of NEK2 expression in different WHO grades of glioma, using the CGGA database. (E) Analysis of NEK2 expression in different WHO grades of glioma, using the CGGA database ($****P < 0.0001$, with one-way ANOVA followed by Tukey's multiple comparison test). (F) Co-expression analysis of CCNA2 and NEK2 expression in GBM, using the CGGA database ($P < 0.0001$, with Pearson correlation coefficient). (G) The Kaplan-Meier analysis of overall survival in patients with glioma based on CCNA2 expression, using the CGGA database ($P < 0.0001$, with log-rank test). (H) The Kaplan-Meier analysis of overall survival in patients with GBM based on CCNA2 expression, using the CGGA database ($P = 0.012$, with log-rank test). (I) Kaplan-Meier analysis of overall survival in patients with glioma based on NEK2 expression, using the CGGA database ($P < 0.0001$, with log-rank test). (J) The Kaplan-Meier analysis of overall survival in patients with GBM based on NEK2 expression, using the CGGA database ($P = 0.026$, with log-rank test). (K) The Kaplan-Meier analysis of overall survival in patients with glioma and GBM based on CCNA2 and NEK2 expression, using the CGGA database ($P < 0.0001$, for all glioma and $P = 0.013$, for GBM, respectively, with log-rank test). (L) Immunohistochemical staining of CCNA2 and NEK2 in GBM samples, compared with adjacent normal tissue. (M) Protein expression of CCNA2 and NEK2 in GBM samples, compared with adjacent normal tissue. T, tumor tissue; N, adjacent normal tissue. Original blots are presented in Fig. S1. Western blot and immunohistochemical analyses were conducted to detect CCNA2 and NEK2 protein levels in GBM samples ($*P < 0.05$, $**P < 0.01$, $***P < 0.001$ and $****P < 0.0001$, with independent t-test). Data represent the mean \pm SD of triplicate determinations from three independent experiments. CCNA2, cyclin A2; NEK2, NIMA related kinase 2; WHO, World Health Organization; TCGA, The Cancer Genome Atlas; GBM, glioblastoma; CGGA, Chinese Glioma Genome Atlas.

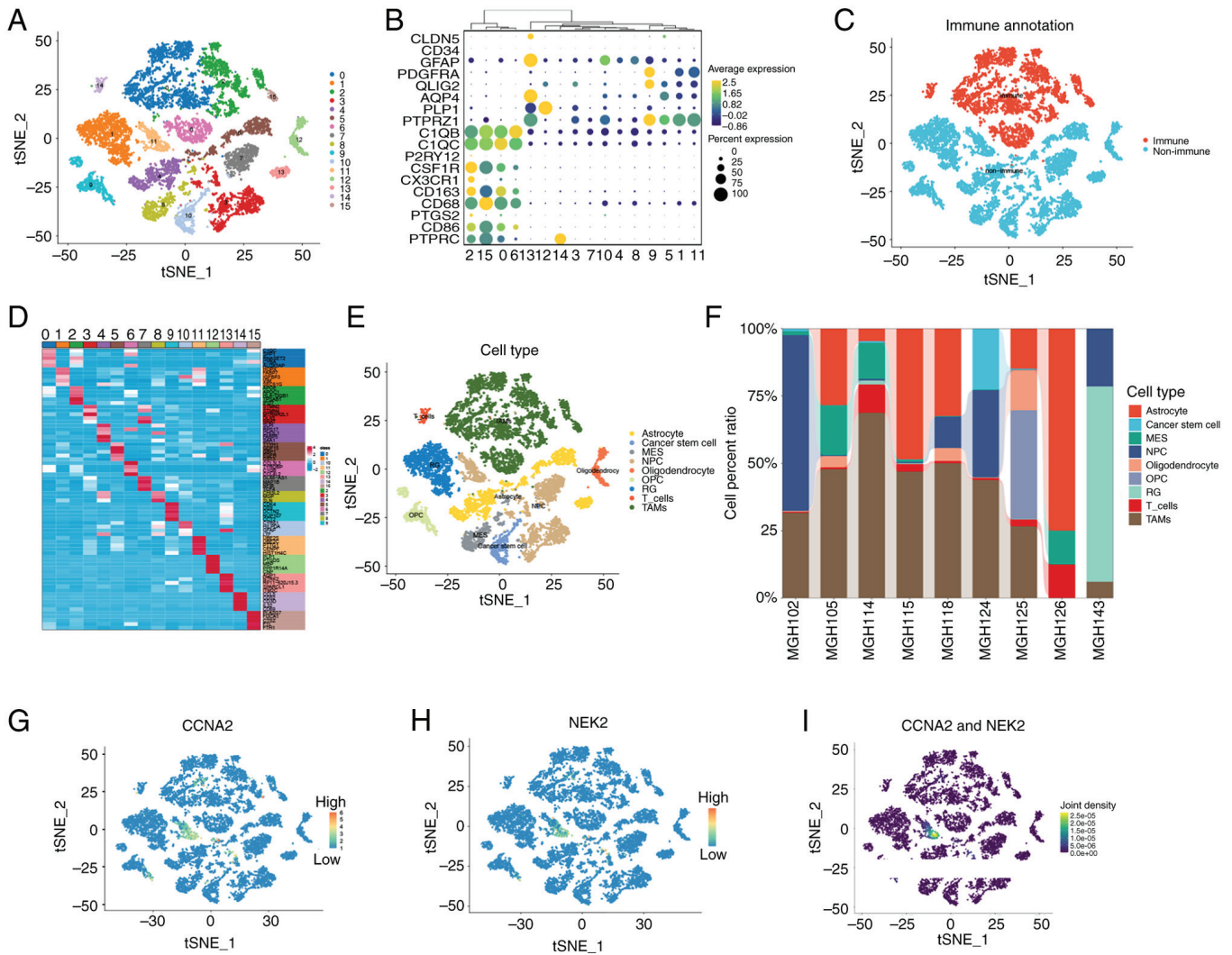


Figure 2. CCNA2 and NEK2 are co-expressed in neural progenitor cell subtypes. (A) GBM cells from nine patients were clustered into 16 distinct groups, using t-SNE dimensionality reduction (colors indicate clusters). (B) Immune and non-immune marker genes of 16 clusters are shown, using bubble plots. (C) Annotation of immune and non-immune cells in single-cell datasets, using t-SNE. (D) Marker genes were identified as the top five differential genes in 16 clusters. (E) Identification of nine distinct cell types out of the 16 clusters. (F) Cell type distribution among nine patients. (G) Distribution of CCNA2 expression across nine cell types. (H) Distribution of NEK2 expression across nine cell types. (I) Distribution of co-expression of CCNA2 and NEK2 across nine cell types. CCNA2, cyclin A2; NEK2, NIMA related kinase 2; GBM, glioblastoma; t-SNE, t-distributed stochastic neighbor embedding.

The trajectory of GBM cell states reveals branched progression. Based on the aforementioned results, it was found that NPCs showed a higher level of stemness, indicating that these cell types may contribute to the initiation and progression of GBM. In addition, CCNA2 and NEK2 expression levels significantly increased in NPCs. To comprehend the function of CCNA2 and NEK2 in GBM, the pseudo-time analysis was utilized to delineate the differentiation pathways of astrocytes and NPCs from the ‘MGH143’ patient, employing the Monocle 2 package. As depicted in Fig. 4A and B, it was observed that astrocytes and NPCs followed a trajectory of differentiation with two branched progressions originating from NPCs. It was observed that NPCs were mainly in the first half of pseudo-time trajectory, whereas astrocytes were mainly in the second half. Furthermore, NPCs highly expressed CCNA2 and NEK2, which were related to cell cycle. It was hypothesized that NPCs may differentiate into astrocytes, but the specific differentiation mechanism remains

unclear. Furthermore, when examining the different clusters, it was observed that clusters 3 and 4 (NPCs) were primarily located in the starting position, whereas the remaining clusters were dispersed throughout various time periods (Fig. S3). This supported the hypothesis that NPC contributes to the onset of GBM. Moreover, as demonstrated in Fig. 4C, it can be observed that CCNA2 and NEK2 expression levels were higher at the beginning and end stages of GBM and exhibited a ‘U’-shaped pattern of distribution (Fig. 4D). It was hypothesized that CCNA2 and NEK2-highly expressing NPCs may have an advantage to grow in the middle and later development of GBM, which has polyclonal sources (67), but it requires further research to investigate it.

As aforementioned, astrocytes and NPCs follow two different paths at a distinct bifurcation point. According to earlier studies, cells on different trajectories exhibit distinct cellular functions or procedural changes. Therefore, analyzing bifurcation points in cells will help understand

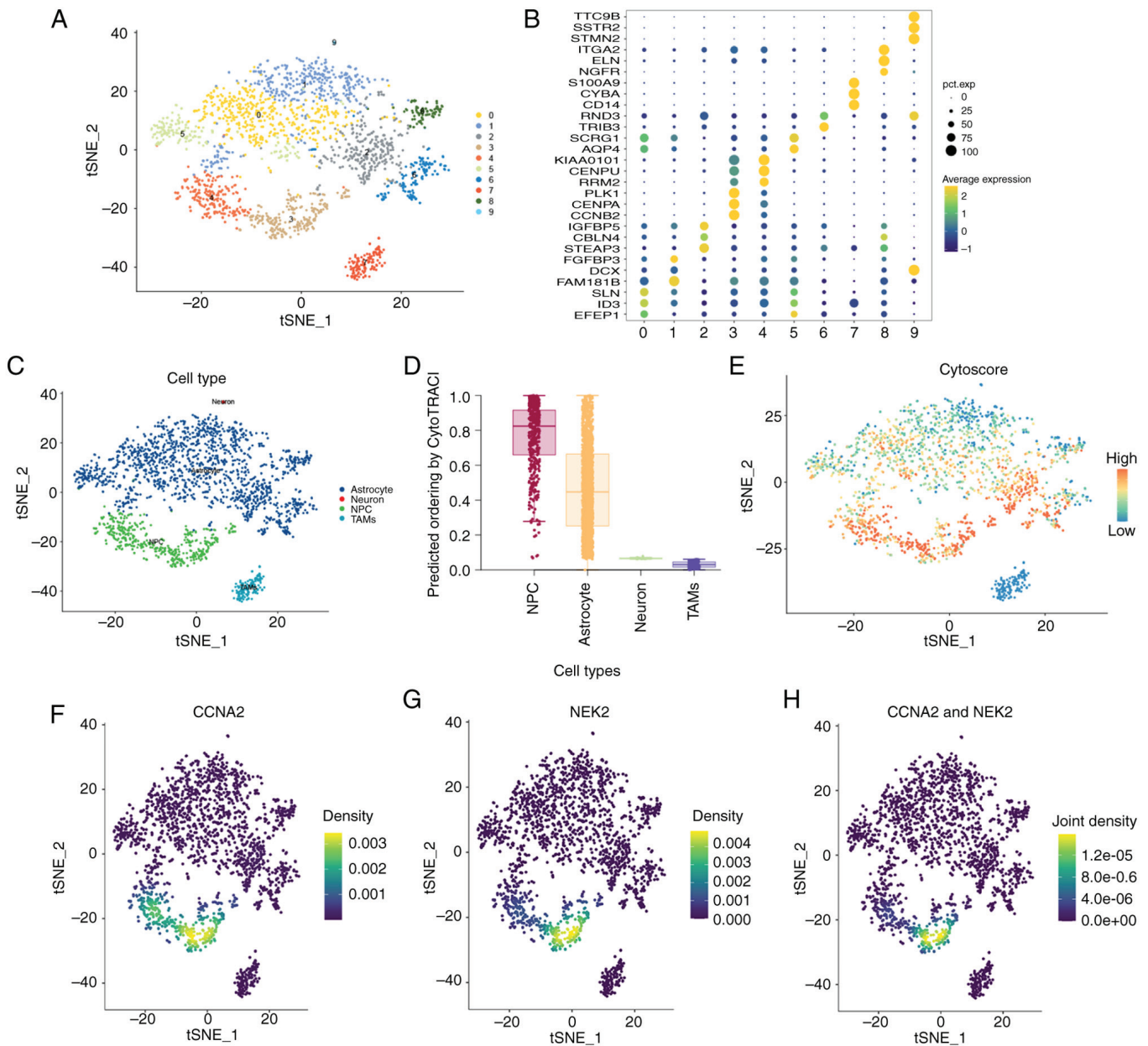


Figure 3. Neural progenitor cells exhibit significant stemness in GBM. (A) GBM cells from patient ‘MGH143’ patient were clustered into 10 distinct groups using t-SNE dimensionality reduction (colors indicate clusters). (B) Marker genes were identified as the top three differential genes in each cluster. (C) Identification of four distinct cell types out of 10 clusters. (D) Proliferation and differentiation potential of four cell types were evaluated using the CytoTRACE package. (E) The stemness/differentiation score was assessed by the CytoTRACE algorithm. (F) Distribution of CCNA2 expression among four cell types. (G) Distribution of NEK2 expression among four cell types. (H) Distribution of co-expression of CCNA2 and NEK2 among four cell types. GBM, glioblastoma; t-SNE, t-distributed stochastic neighbor embedding; CCNA2, cyclin A2; NEK2, NIMA related kinase 2.

the underlying genes responsible for these changes (68,69). The BEAM analysis was performed on this bifurcation point, resulting in the clear division of 1,542 genes into three clusters with distinct expression patterns. Cluster 3 comprises 190 genes, including CCNA2 and NEK2, which were found to be overexpressed in the primary stage, based on a branched expression pattern in pseudo-time dimension. This suggested that these genes may play a role in the progression of GBM (Fig. 4E). Furthermore, the GSEA analysis revealed that these clusters exhibited distinct functions. Specifically, cluster 3 was associated with chromosome segregation, mitotic nuclear division, sister chromatid segregation, nuclear chromosome segregation

and nuclear division (Fig. 4F), which are related to the cell cycle.

GBM prognosis may be associated with P-NPCs. As aforementioned (Figs. 2 and 4), CCNA2 and NEK2 were co-expressed in a group of early active cells known as NPCs. To investigate the clinical significance of these cells in patients with GBM, marker genes that were differentially expressed between P-NPCs and negative cells in the patient ‘MGH143’ were identified (Fig. 5A). The ‘AddModuleScore’ was utilized to assess all single-cell datasets and validate the suitability of marker genes (Fig. S4). The results were consistent with those shown in Fig. 2I, thus indicating that

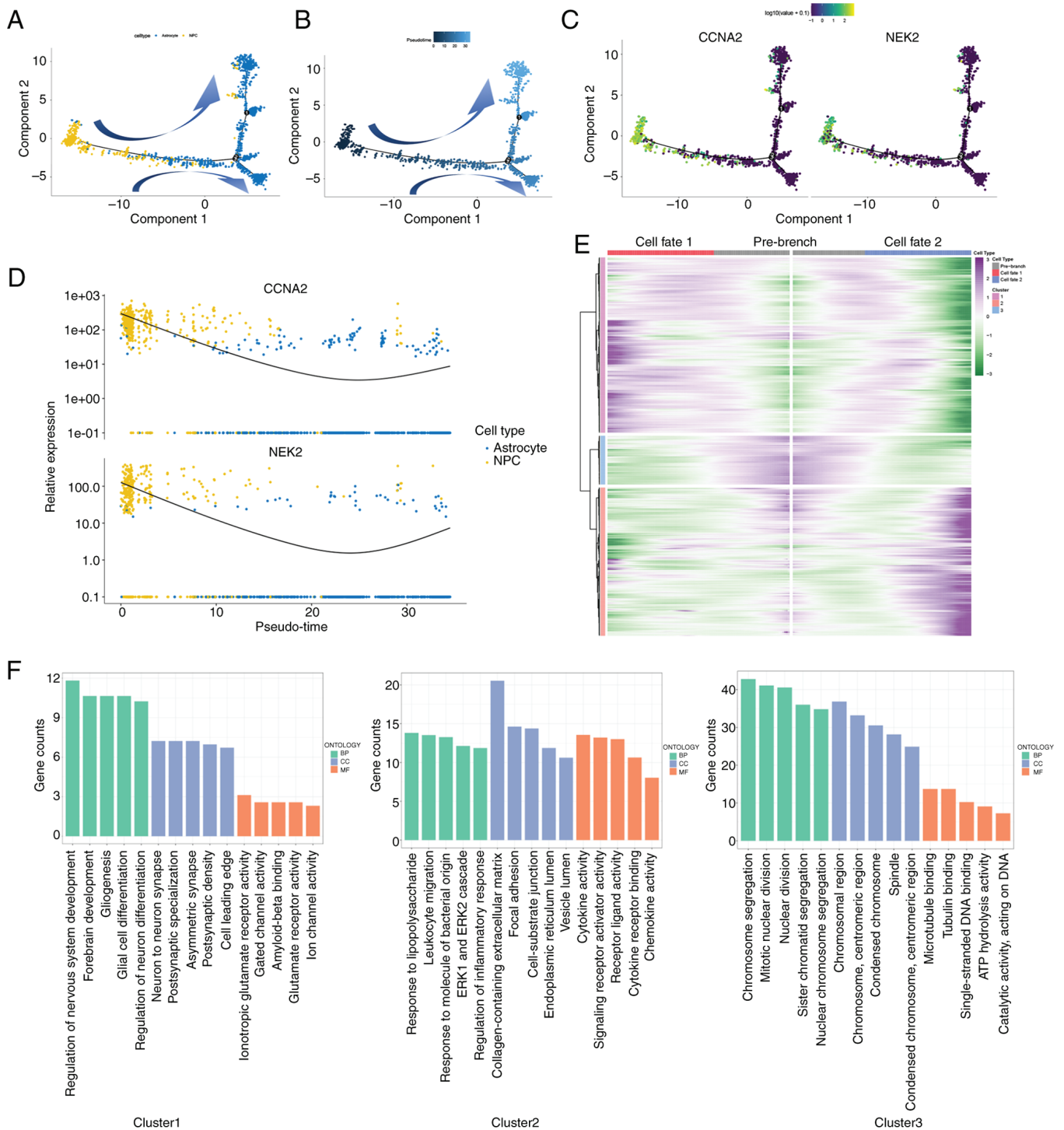


Figure 4. The trajectory of GBM cell states reveals branched progression. (A) Differentiation pathways of astrocytes and NPCs from patient 'MHG143'. (B) Pseudo-time analysis to delineate the differentiation pathways of astrocytes and NPCs from patient 'MHG143'. (C) Pseudo-time trajectory of the expression of CCNA2 and NEK2 in NPCs and astrocytes. (D) Tendency of CCNA2 and NEK2 expression with pseudo-time trajectory. (E) CCNA2 and NEK2 overexpression in the primary stage, based on a branched expression pattern in pseudo-time dimension. (F) The gene set enrichment analysis revealed that three clusters exhibited distinct functions. GBM, glioblastoma; NPCs, neural progenitor cells; CCNA2, cyclin A2; NEK2, NIMA related kinase 2.

this set of genes accurately represents P-NPCs. Subsequently, ssGSEA was employed to investigate the expression of marker genes in gliomas of varying grades in the CGGA database. Results indicated a significant difference in expression levels with increasing WHO grades, as demonstrated in Fig. 5B. Comparable results were observed in TCGA database (Fig. 5C). As revealed in Fig. 5D, the goodness-of-fit

was investigated, and the results indicated that the proportion of P-NPCs was more appropriate in GBM, suggesting that P-NPCs may be more representative in GBM. The Kaplan-Meier analysis demonstrated that patients with high expression of marker genes exhibited a shorter overall survival in GBM and gliomas of all grades (Fig. 5E). These results indicated that marker genes, which may represent

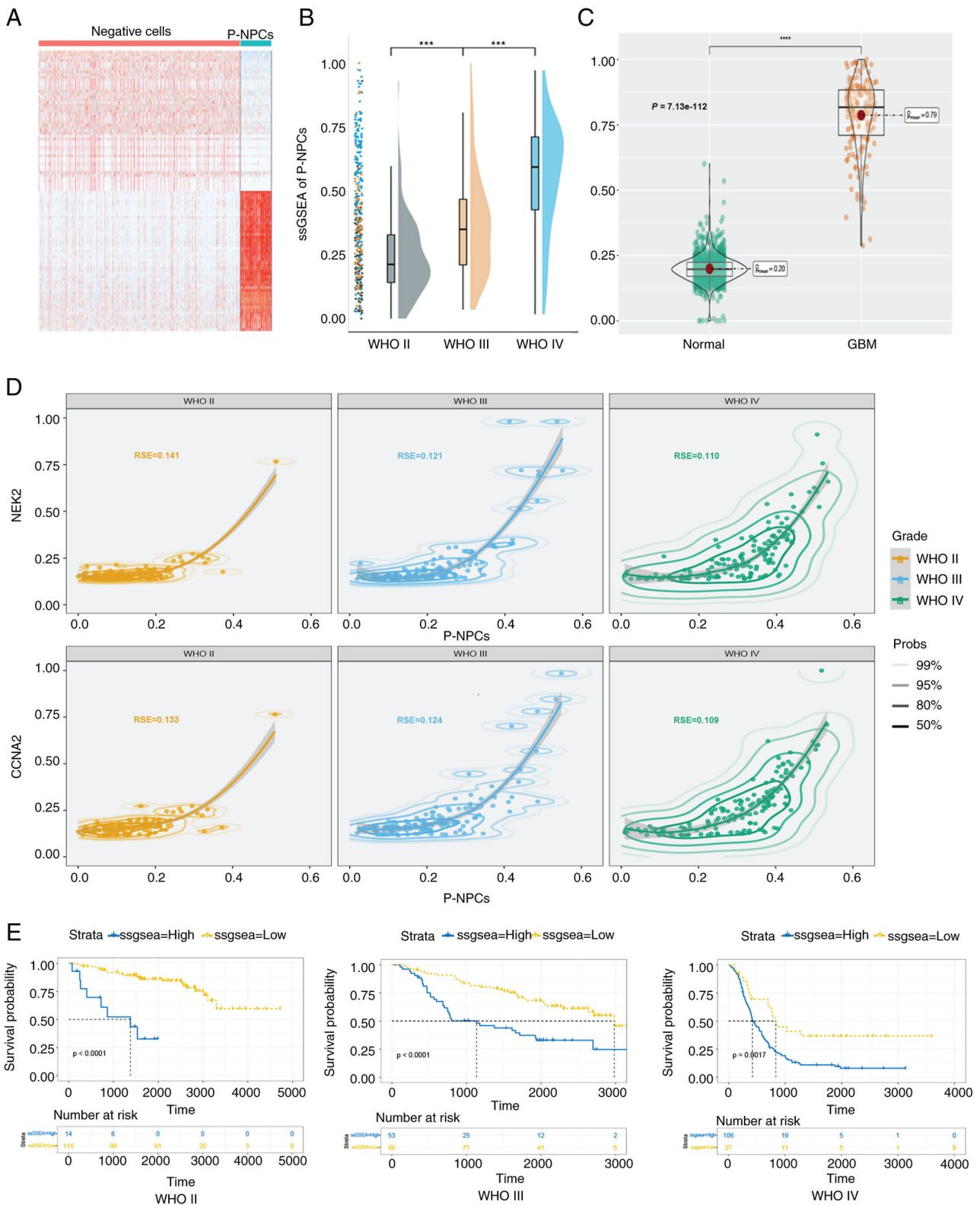


Figure 5. GBM prognosis may be associated with P-NPCs. (A) Heatmap of gene expression differences between negative-cells and P-NPCs. (B) ssGSEA score of P-NPCs in the Chinese Glioma Genome Atlas database across various grades of glioma (** $P < 0.001$, with independent t-test). (C) The ssGSEA score of P-NPCs derived from both normal and GBM patient samples in The Cancer Genome Atlas database (**** $P < 0.0001$, with independent t-test). (D) Suitability of P-NPCs and CCNA2 and NEK2 expression in glioma grades. (E) Association of high expression of marker genes with shorter overall survival in patients with glioma, according to the Kaplan-Meier analysis ($P < 0.0001$ for WHO II, $P < 0.0001$ for WHO III and $P = 0.0017$ for WHO IV, respectively, with log-rank test). GBM, glioblastoma; P-NPCs: positive neural progenitor cells; ssGSEA, single-sample gene set enrichment analysis; CCNA2, cyclin A2; NEK2, NIMA related kinase 2; WHO, World Health Organization.

P-NPCs, may be utilized to differentiate the WHO grade of GBM patients and assess their prognosis.

P-NPCs are associated with the co-expression of CCNA2 and NEK2 in the G2M checkpoint pathway. Based on the

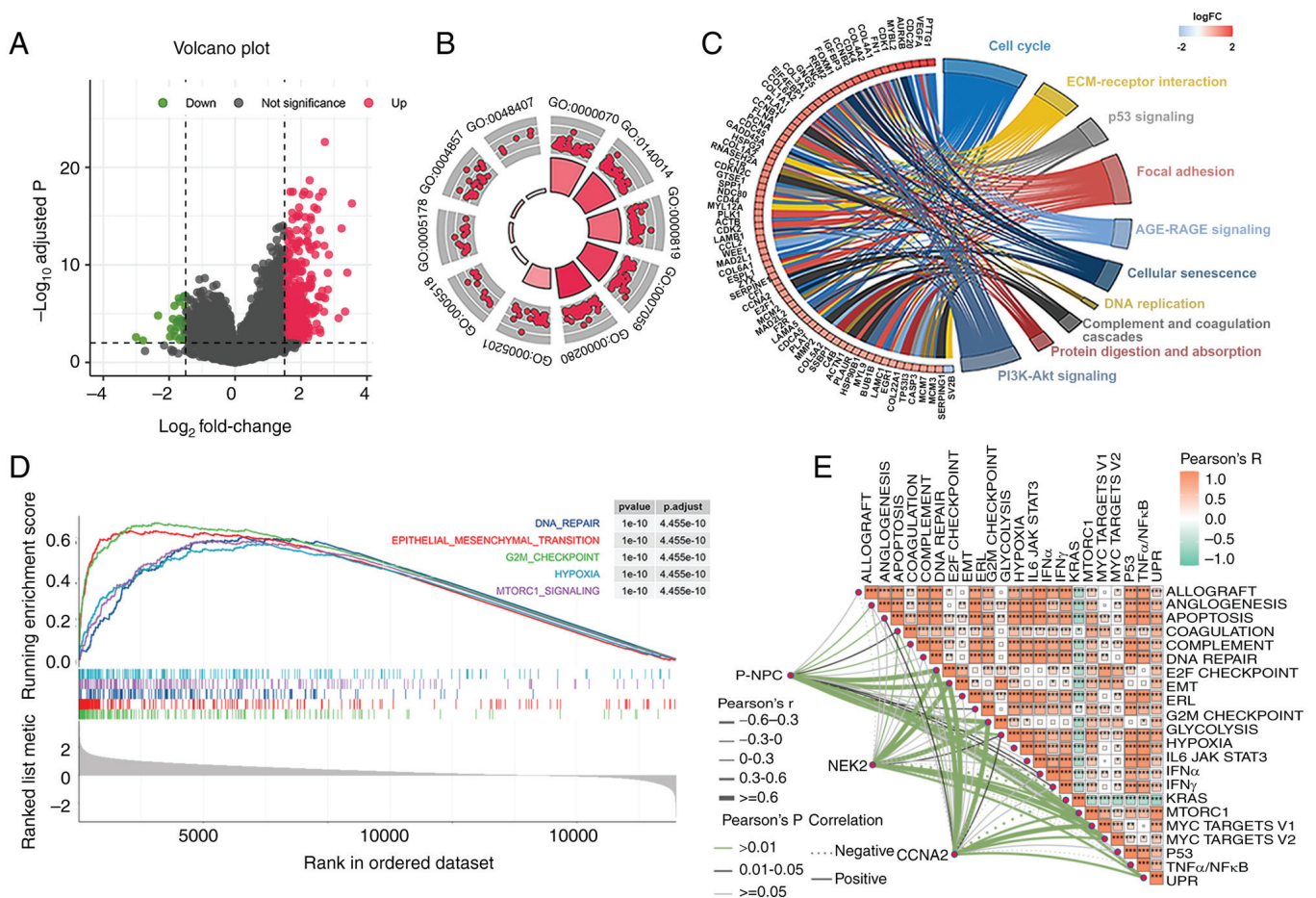


Figure 6. P-NPCs are associated with the co-expression of CCNA2 and NEK2 in the G2M checkpoint pathway. (A) Identification of upregulated genes in patients with GBM with different prognoses in a volcano plot, based on \log_2 FC >1.5 and an adjusted P-value <0.05. (B) Gene Ontology analysis of DEGs. (C) The Kyoto Encyclopedia of Genes and Genome analysis of DEGs. (D) The GSEA analysis revealed five pathways significantly activated in patients with poor survival. (E) A correlation was found between the single-sample GSEA score of P-NPCs and the expression of CCNA2 and NEK2 in the G2M checkpoint pathway (* P <0.05, ** P <0.01 and *** P <0.001, with independent t-test). CCNA2, cyclin A2; NEK2, NIMA related kinase 2; GBM, glioblastoma; DEGs, differentially expressed genes; GSEA, gene set enrichment analysis; P-NPC, positive neural progenitor cell.

forementioned survival analysis for patients with GBM in the CGGA database (Fig. 5), a total of 27 patients with poor survival and 106 patients with improved survival rates were observed. An analysis of DEGs in patients with varying prognoses was then conducted. Results indicated that 455 genes were significantly upregulated, whereas 29 genes were significantly downregulated (Fig. 6A). Enrichment analysis of GEO and KEGG pathways for the DEGs indicated that the low survival rate of patients with GBM was associated with increased activity in mitosis and cell cycles (Fig. 6B and C). Subsequently, the GSEA analysis revealed that five pathways, namely DNA repair, epithelial-mesenchymal transition, G2M checkpoint, hypoxia and MTORC1 signaling, were significantly activated in patients with poor survival (Fig. 6D). To validate the aforementioned results, ssGSEA analysis was utilized to reevaluate them. As a result, a total of 23 pathways, which included the five aforementioned pathways, were found to be significantly enriched (Fig. S5). Furthermore, a correlation between the ssGSEA score of P-NPCs and the expression of CCNA2 and NEK2 in the G2M checkpoint pathway was observed (Fig. 6E). These results suggested that the differential prognosis of these patients may be related to the role of P-NPCs in driving the cell cycle and that the G2M checkpoint may be a key factor in these differences.

G2M checkpoint pathway is activated in P-NPCs. NPCs from patient 'MGH143' exhibited high activity levels, but the specific functions of the other cells remain unclear. To further examine the underlying pathways in scRNA-seq, TAMs and neurons were removed. Next, the marker genes of the remaining eight clusters were used to conduct significant differential pathway analysis through GSEA. As a result, hallmark pathways were significantly enriched, including mTORC1, hypoxia, Myc-targets-v1, TNF α -signaling-via-NF- κ B and G2M checkpoint (Fig. 7A). The top four pathways (mTORC1, cell cycle, oxidative, and NF- κ B) were selected to generate butterfly plots, based on the enrichment score of each cluster (Fig. 7B). Clusters 3 and 4 belonged to NPCs, as demonstrated in Fig. 3C. These clusters revealed a strong proliferation of E2F targets and G2M checkpoints, as depicted in Fig. 7A. Furthermore, they were assigned to cell cycle quadrants, as illustrated in Fig. 7B. However, they were not equally distributed among the four quadrants. Cluster 3, as compared with cluster 4, exhibited significantly enriched pathways, including the mitotic spindle and the G2M checkpoint (Fig. 7C). This indicated a stronger association with the cell cycle. The tricycle analysis (37) was used to evaluate the cell cycle position of single-cell data from patients. The position of cells in the cell cycle was denoted

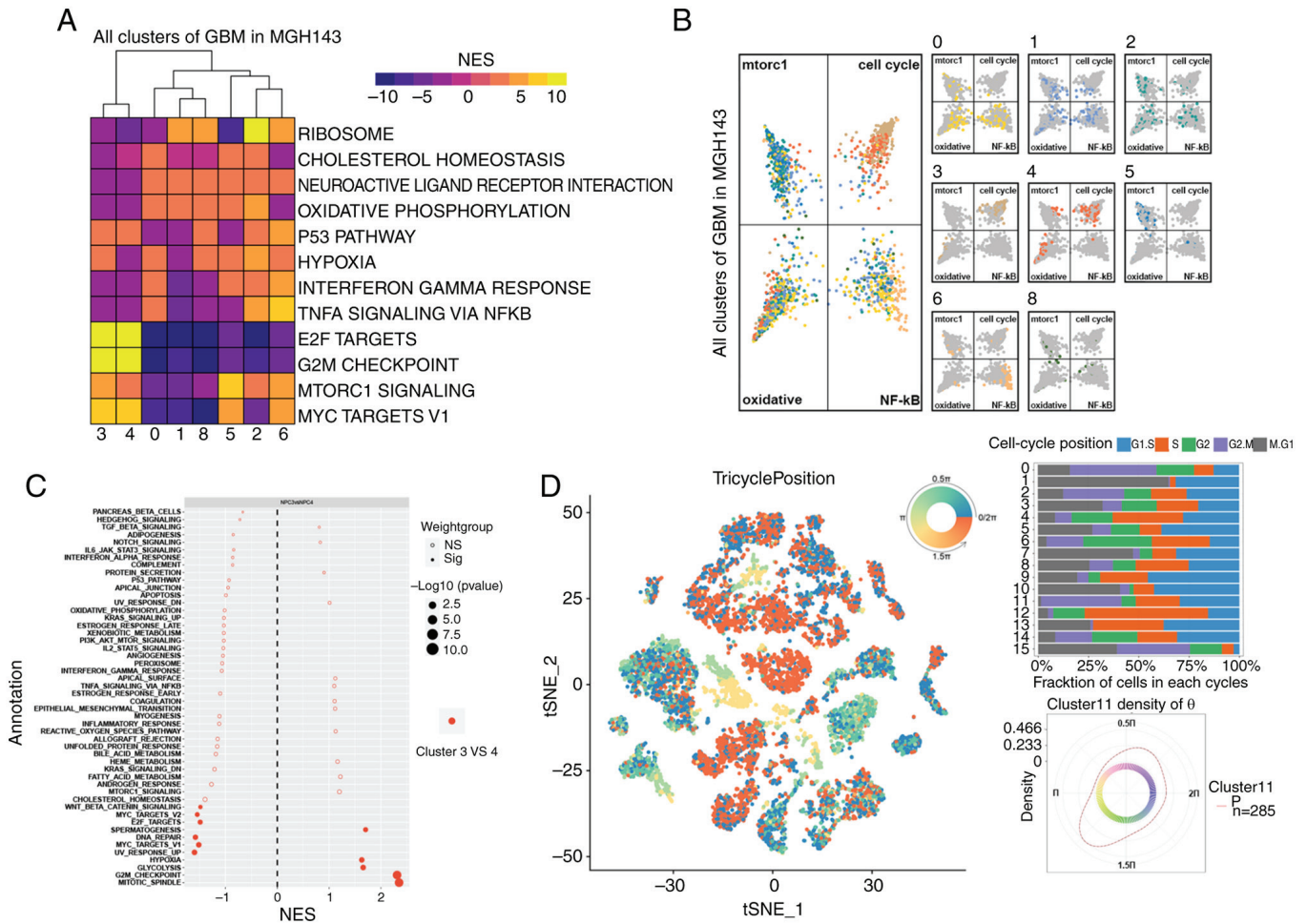


Figure 7. Activation of the G2M checkpoint pathway in positive neural progenitor cells. (A) Hallmark pathways, including mTORC1, hypoxia, Myc-targets-v1, TNF α -signaling-via-NF- κ B and G2M checkpoint, were enriched. (B) Four pathways (mTORC1, cell cycle, oxidative and NF- κ B) were selected for butterfly plots based on cluster enrichment scores. (C) Cluster 3 had enriched pathways, including mitotic spindle and G2M checkpoint, as compared with cluster 4. (D) Tricycle analysis of the cell cycle position of single-cell data. GBM, glioblastoma; t-SNE, t-distributed stochastic neighbor embedding; NES, normalized enrichment score.

by an angle θ and cells in the same stage always appeared at a similar θ . To accurately represent the position of cells in the cell cycle, a circular color scale that considers the circular nature of the cell cycle was utilized, with positions ‘wrap around’ from 0 to 2π (Fig. 7D). For instance, cells at the G2/M stage are represented by colors centered at 1.75π (Fig. 7D). It was revealed that cluster 11 (NPCs) accounted for a high proportion of cells in the G2/M phase (Fig. 7D). In general, NPCs or a subset of them (cluster 3) were strongly enriched at the G2M checkpoint. These cells may contribute to GBM cell population proliferation and disease progression.

Establishment and evaluation of a nomogram with the TCGA dataset. The forest plot presented P-NPCs, age and chemotherapy score as independent risk factors (Fig. S6). As radiotherapy has been widely used in clinical practice and its effectiveness has been previously reported in the literature (70,71), it was included in the present study. The Schoenfeld residual test indicated that all variables equally satisfied the assumption of proportional hazards (Fig. S6). Outliers were not observed, based on the deviance residual test (Fig. S6). After considering all the aforementioned significant

predictive factors, a comprehensive nomogram that includes P-NPCs, age, chemotherapy and radiotherapy score was developed (Fig. 8A). The calibration curves for one, two and three years revealed a satisfactory calibration efficiency. A closer alignment with the dashed line indicated an improved prediction performance (Fig. 8B). The DCA was used to evaluate the clinical application of the nomogram and the net benefit of various prediction models at different threshold probabilities. This was achieved by weighing the benefits against the harms and minimizing the latter. The comprehensive nomogram demonstrated a more favorable probability and an improved net benefit compared with P-NPCs and clinical index, as shown in Fig. 8C-E. Subsequently, the nomogram score model and clinical index score model were evaluated using the concordance index. Results demonstrated that the nomogram score had a higher prediction accuracy than the clinical index score (Fig. 8F). Furthermore, the time-dependent ROC curve analysis demonstrated that the predictive performance of the nomogram gradually improved over time (Fig. 8G). The Kaplan-Meier analysis indicated that a higher nomogram score was associated with a poorer prognosis for patients with GBM (Fig. 8H). Therefore, a comprehensive nomogram was

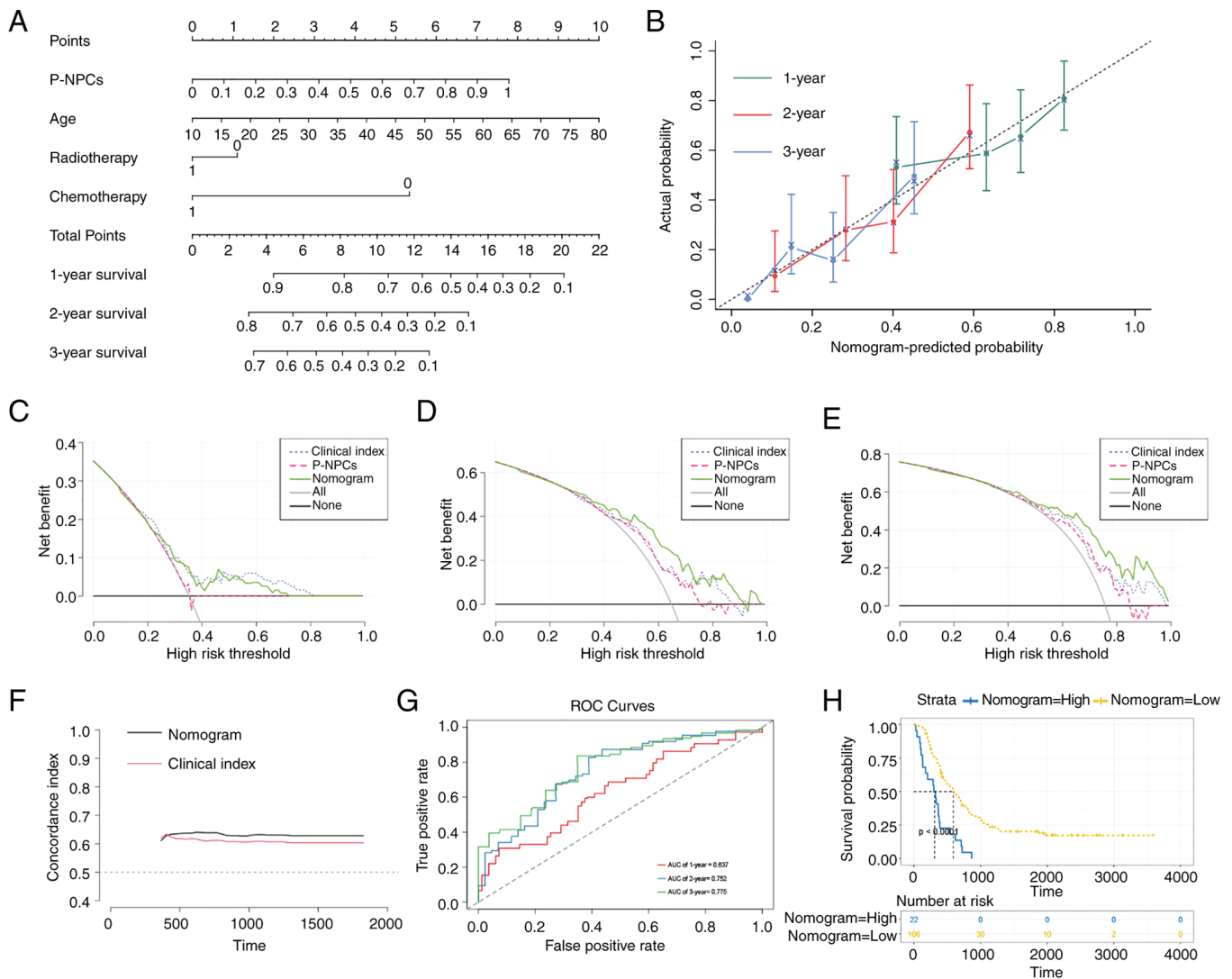


Figure 8. Establishment and evaluation of a nomogram with TCGA dataset. (A) A nomogram predicts 1-, 2- and 3-year overall survival probability in GBM by considering P-NPCs, age, chemotherapy and radiotherapy scores. (B) The calibration curves for 1, 2 and 3 years showed improved calibration potential in TCGA cohort. The black dotted lines represent the ideal predictive model, whereas the solid lines represent the nomogram models for each respective year. (C-E) The decision curve analysis was used to evaluate the clinical application of the nomogram and the net benefit of various prediction models when the threshold probability is between 0 and 0.80. (F) The concordance index was used to evaluate the accuracy and discrimination of the nomogram's predicted values vs. the clinical index model. (G) Time-dependent ROC curve analysis was conducted for the nomogram at 1, 2 and 3 years in TCGA cohort. (H) The Kaplan-Meier analysis found that higher nomogram scores were linked to poorer prognosis in patients with GBM ($P < 0.0001$ with log-rank test). TCGA, The Cancer Genome Atlas; GBM, glioblastoma; P-NPCs, positive neural progenitor cells; ROC, receiver operating characteristic.

established based on multiple prognostic factors that exceeded the predictive power of each factor alone. The nomogram may assist clinicians in making more precise assessments of patient prognosis.

Discussion

The cell cycle, a complex process tightly regulated by various proteins (67), is closely linked to the development and advancement of cancer (72,73). NEK2 is a member of the NIMA-related family of serine/threonine protein kinases, which are considered to play a role in regulating the cell cycle (74). Upregulation of NEK2 in human cells leads to premature splitting of the centrosome, whereas overexpression of a NEK2 kinase-dead mutant results in centrosome abnormalities and aneuploidy (10,75). These factors are

significant contributors to tumorigenesis (76). NEK2 has two splice variants, namely NEK2A and NEK2B. NEK2A is necessary for centrosome separation during the G2/M transition (77). The abnormal expression of NEK2A may play a role in regulating genetic stability and tumorigenesis. In the present study, a positive correlation was observed between the expression of CCNA2 and NEK2 and the progression of glioma. Furthermore, CCNA2 and NEK2 were upregulated in a subset of P-NPCs in GBM, which exhibited significant proliferation and progression properties. CCNA2 is located on chromosome 4 and is encoded by the human CCNA2 gene. Belonging to the highly conserved cyclin family, this protein promotes progression through the S-phase and transition from G2 to M phase by binding to CDK in the mitotic cell cycle (78). Jiang *et al* (79) proposed that CCNA2 promotes proliferation, migration, invasion and regulates macrophage polarization in

glioma. It is recognized that changes in cell cycle proteins may trigger cancer. CCNA2 and NEK2 are classified as cell cycle regulatory genes, which are crucial in the advancement and prognosis of pancreatic cancer (28). However, the correlation and underlying mechanism between CCNA2 and NEK2 has not been fully explored in GBM. The present study presented a novel finding on the co-expression of CCNA2 and NEK2 in GBM and their association with NPCs, thus suggesting their involvement in regulating the cell cycle.

GBM are the most common malignant tumors in the nervous system, which are known for their rapid progression and short survival rates (80,81). Therapeutic approaches for GBM have slowly progressed, unlike other multimodal therapies for tumors (82). Ongoing efforts are being made to understand the highly heterogeneous nature of GBM. Differences have been observed among various tumor types, individuals with identical diagnoses, non-tumor cell types and states and individual tumor cell clones (83). NPCs are the precursor cells of the central nervous system (CNS) that generate many, if not all, of the glial and neuronal cell types that populate the CNS (84). It has been proposed that NPCs are the preferred cell of origin for GBM (85). In addition, NPCs have a strong potential to migrate (86), renew (87) and maintain the population (88,89). In the present study, patients with GBM were analyzed at the single-cell level and it was discovered that CCNA2 and NEK2 were co-expressed in NPCs. These findings suggested that they may have a significant role in the development and progression of GBM. Furthermore, the abundance of NPCs in patient 'MGH143' was higher during the initial stages of tumorigenesis and was similar to the peak expression of CCNA2 and NEK2. Therefore, it was hypothesized that changes in CCNA2 and NEK2 may drive the progression of NPCs and ultimately contribute to the development of GBM. CCNA2 and NEK2 were found to be differentially expressed in NPC subtypes, indicating cellular heterogeneity in the glioma-associated microenvironment. This finding agrees with previous research on NPCs heterogeneity (90).

In the present study, NPCs exhibiting high expression levels of CCNA2 and NEK2 as P-NPCs were defined. Moreover, the marker genes based on P-NPCs significantly distinguish the prognosis of patients with GBM. In GBM, NPCs highly expressed stemness-associated cell membrane antigens such as CD133, CD15/SSEA, CD44, or A2B5 and intracellular markers such as Sox2 and Nestin (91,92) and have demonstrated the potential for cellular transitions (31). Similar to normal neurogenesis processes, NPCs may generate more differentiated phenotypes with astrocytic features in GBM (91). As aforementioned, CCNA2 and NEK2 are closely related to the cell cycle, which is responsible for cell differentiation and fate (93). The origin of glioma cells is polyclonal (40) and in the development of cancer, the population with competitive advantages will be selected to develop (94). Therefore, it was hypothesized by the authors that CCNA2 and NEK2 are only expressed in some NPC subtypes, which may have a competitive advantage, but the specific process requires further discussion. In the analysis of different pathways among these patients with varying prognoses, it was found that the G2M checkpoint was highly enriched. The G2/M checkpoint prevents cells with damaged DNA from entering mitosis, allowing repair of DNA that was damaged during the late S or

G2 phases before mitosis. A weakened G2/M checkpoint under therapeutic conditions may trigger cell death through mitotic catastrophe in cells with irreparable DNA damage and faulty mitotic machinery (95). It was revealed that the G2M checkpoint is significantly increased in patients with poor prognosis. This increase may inhibit mitotic catastrophe, which in turn promotes rapid tumor growth. Currently, there are numerous drugs that target the G2M checkpoint (96). The present study may offer a novel approach to the pharmacological mechanism. By recognizing the significance of P-NPCs, a comprehensive nomogram that incorporates clinical characteristics to predict patient prognosis more accurately has been developed.

However, the data on the regulatory relationship between NEK2 and CCNA2 expression in GBM are limited, which cannot accurately reflect the heterogeneity of glioma. At the same time, single-cell sequencing loses the information of spatial location, thus it is impossible to characterize their co-localization relationship in spatial location. Mapping research through multiple samples will be conducted. Moreover, the authors have marginal information on the regulatory association between CCNA2 and NEK2 in GBM and the role they play in different stages of the cell cycle is unclear, thus more experiments are needed to determine their regulatory role in GBM. To date, it is not feasible to precisely determine the composition of these cells before surgery. This information is only inferred through postoperative sequencing. To address this practical issue, a non-invasive preoperative assessment method should be developed for these cells.

Acknowledgements

Not applicable.

Funding

The present study was supported by the National Natural Science Foundation of China (grant nos. 82072781 and 81602207) and Medical Foundation-Clinical Integration Program of Xi'an Jiaotong University (grant no. YXJLRH2022040).

Availability of data and materials

The datasets used and/or analyzed during the current study are available from the corresponding author on reasonable request.

Authors' contributions

MDW and PM conceptualized and designed the study. HYZ, TW and WW developed methodology. HYZ, WW, YYC and YCW acquired data. HYZ, BCZ and WW analysed and interpreted the data. HYZ, WW and YYC wrote the manuscript. YYC performed experiments. HYZ and YCW confirm the authenticity of all the raw data. All authors read and approved the final version of the manuscript.

Ethics approval and consent to participate

The WHO grade II, III and IV gliomas were obtained from patient samples with a pathological diagnosis who underwent craniotomy at the First Affiliated Hospital of Xi'an Jiao

Tong University (Shaanxi, China). The research involving the utilization of these biological specimens received ethical approval from the Ethics Committee of the hospital located in Xi'an, Shaanxi, China (approval no. XJTU1AF2022LSK-428). Informed consent was obtained through the signing of consent forms for the utilization of clinical samples, all experimental protocols used in the present study were in accordance with the guidelines of the Declaration of Helsinki.

Patient consent for publication

Not applicable.

Competing interests

The authors declare that they have no competing interests.

References

- Ostrom QT, Price M, Neff C, Cioffi G, Waite KA, Kruchko C and Barnholtz-Sloan JS: CBTRUS statistical report: Primary brain and other central nervous system tumors diagnosed in the United States in 2015-2019. *Neuro Oncol* 24 (Suppl 5): v1-v95, 2022.
- Xu S, Tang L, Li X, Fan F and Liu Z: Immunotherapy for glioma: Current management and future application. *Cancer Lett* 476: 1-12, 2020.
- Liu Y, Lang F and Yang C: NRF2 in human neoplasm: Cancer biology and potential therapeutic target. *Pharmacol Ther* 217: 107664, 2021.
- Asad AS, Candia AJN, González N, Zuccato CF, Seilicovich A and Candolfi M: Current non-viral gene therapy strategies for the treatment of glioblastoma. *Curr Med Chem* 28: 7729-7748, 2021.
- Shergalis A, Bankhead A III, Luesakul U, Muangsin N and Neamati N: Current challenges and opportunities in treating glioblastoma. *Pharmacol Rev* 70: 412-445, 2018.
- Huang PH, Xu AM and White FM: Oncogenic EGFR signaling networks in glioma. *Sci Signal* 2: re6, 2009.
- Liu H, Liu B, Hou X, Pang B, Guo P, Jiang W, Ding Q, Zhang R, Xin T, Guo H, *et al*: Overexpression of NIMA-related kinase 2 is associated with poor prognoses in malignant glioma. *J Neurooncol* 132: 409-417, 2017.
- Xiang J, Alafate W, Wu W, Wang Y, Li X, Xie W, Bai X, Li R, Wang M and Wang J: NEK2 enhances malignancies of glioblastoma via NIK/NF- κ B pathway. *Cell Death Dis* 13: 58, 2022.
- Xia J, Franqui Machin R, Gu Z and Zhan F: Role of NEK2A in human cancer and its therapeutic potentials. *Biomed Res Int* 2015: 862461, 2015.
- Faragher AJ and Fry AM: Nek2A kinase stimulates centrosome disjunction and is required for formation of bipolar mitotic spindles. *Mol Biol Cell* 14: 2876-2889, 2003.
- Jeong Y, Lee J, Kim K, Yoo JC and Rhee K: Characterization of NIP2/centrobin, a novel substrate of Nek2, and its potential role in microtubule stabilization. *J Cell Sci* 120: 2106-2116, 2007.
- Zhong X, Guan X, Liu W and Zhang L: Aberrant expression of NEK2 and its clinical significance in non-small cell lung cancer. *Oncol Lett* 8: 1470-1476, 2014.
- Gu Z, Xia J, Xu H, Frech I, Tricot G and Zhan F: NEK2 promotes aerobic glycolysis in multiple myeloma through regulating splicing of pyruvate kinase. *J Hematol Oncol* 10: 17, 2017.
- Zhang X, Huang X, Xu J, Li E, Lao M, Tang T, Zhang G, Guo C, Zhang X, Chen W, *et al*: NEK2 inhibition triggers anti-pancreatic cancer immunity by targeting PD-L1. *Nat Commun* 12: 4536, 2021.
- Lee J and Gollahon L: Mitotic perturbations induced by Nek2 overexpression require interaction with TRF1 in breast cancer cells. *Cell Cycle* 12: 3599-3614, 2013.
- Fang Y and Zhang X: Targeting NEK2 as a promising therapeutic approach for cancer treatment. *Cell Cycle* 15: 895-907, 2016.
- Qi C, Lei L, Hu J, Wang G, Liu J and Ou S: Serine incorporator 2 (SERINC2) expression predicts an unfavorable prognosis of low-grade glioma (LGG): Evidence from bioinformatics analysis. *J Mol Neurosci* 70: 1521-1532, 2020.
- Pagano M, Pepperkok R, Verde F, Ansorge W and Draetta G: Cyclin A is required at two points in the human cell cycle. *EMBO J* 11: 961-971, 1992.
- Murphy M, Stinnakre MG, Senamaud-Beaufort C, Winston NJ, Sweeney C, Kubelka M, Carrington M, Bréchet C and Sobczak-Thépot J: Delayed early embryonic lethality following disruption of the murine cyclin A2 gene. *Nat Genet* 15: 83-86, 1997.
- Jiang A, Zhou Y, Gong W, Pan X, Gan X, Wu Z, Liu B, Qu L and Wang L: CCNA2 as an immunological biomarker encompassing tumor microenvironment and therapeutic response in multiple cancer types. *Oxid Med Cell Longev* 2022: 5910575, 2022.
- Wang Y, Zhong Q, Li Z, Lin Z, Chen H and Wang P: Integrated profiling identifies CCNA2 as a potential biomarker of immunotherapy in breast cancer. *Oncotargets Ther* 14: 2433-2448, 2021.
- Li Z, Zhang Y, Zhou Y, Wang F, Yin C, Ding L and Zhang S: Tanshinone IIA suppresses the progression of lung adenocarcinoma through regulating CCNA2-CDK2 complex and AURKA/PLK1 pathway. *Sci Rep* 11: 23681, 2021.
- Gan Y, Li Y, Li T, Shu G and Yin G: CCNA2 acts as a novel biomarker in regulating the growth and apoptosis of colorectal cancer. *Cancer Manag Res* 10: 5113-5124, 2018.
- Cai Y and Yang W: PKMYT1 regulates the proliferation and epithelial-mesenchymal transition of oral squamous cell carcinoma cells by targeting CCNA2. *Oncol Lett* 23: 63, 2022.
- Bendris N, Arsic N, Lemmers B and Blanchard JM: Cyclin A2, Rho GTPases and EMT. *Small GTPases* 3: 225-228, 2012.
- Li J, Ying Y, Xie H, Jin K, Yan H, Wang S, Xu M, Xu X, Wang X, Yang K, *et al*: Dual regulatory role of CCNA2 in modulating CDK6 and MET-mediated cell-cycle pathway and EMT progression is blocked by miR-381-3p in bladder cancer. *FASEB J* 33: 1374-1388, 2019.
- Zhang J, Liu X, Zhou W, Lu S, Wu C, Wu Z, Liu R, Li X, Wu J, Liu Y, *et al*: Identification of key genes associated with the process of hepatitis B inflammation and cancer transformation by integrated bioinformatics analysis. *Front Genet* 12: 654517, 2021.
- Zhou Z, Cheng Y, Jiang Y, Liu S, Zhang M, Liu J and Zhao Q: Ten hub genes associated with progression and prognosis of pancreatic carcinoma identified by co-expression analysis. *Int J Biol Sci* 14: 124-136, 2018.
- Zhao Z, Zhang KN, Wang Q, Li G, Zeng F, Zhang Y, Wu F, Chai R, Wang Z, Zhang C, *et al*: Chinese glioma genome atlas (CGGA): A comprehensive resource with functional genomic data from Chinese glioma patients. *Genomics Proteomics Bioinformatics* 19: 1-12, 2021.
- Cancer Genome Atlas Research Network; Weinstein JN, Collisson EA, Mills GB, Shaw KR, Ozenberger BA, Ellrott K, Shmulevich I, Sander C and Stuart JM: The cancer genome atlas pan-cancer analysis project. *Nat Genet* 45: 1113-130, 2013.
- Neffel C, Laffy J, Filbin MG, Hara T, Shore ME, Rahme GJ, Richman AR, Silverbush D, Shaw ML, Hebert CM, *et al*: An integrative model of cellular states, plasticity, and genetics for glioblastoma. *Cell* 178: 835-849.e21, 2019.
- Satija R, Farrell JA, Gennert D, Schier AF and Regev A: Spatial reconstruction of single-cell gene expression data. *Nat Biotechnol* 33: 495-502, 2015.
- Aran D, Looney AP, Liu L, Wu E, Fong V, Hsu A, Chak S, Naikawadi RP, Wolters PJ, Abate AR, *et al*: Reference-based analysis of lung single-cell sequencing reveals a transitional profibrotic macrophage. *Nat Immunol* 20: 163-172, 2019.
- Hu C, Li T, Xu Y, Zhang X, Li F, Bai J, Chen J, Jiang W, Yang K, Ou Q, *et al*: CellMarker 2.0: An updated database of manually curated cell markers in human/mouse and web tools based on scRNA-seq data. *Nucleic Acids Res* 51 (D1): D870-D876, 2023.
- Zhang Z, Wang ZX, Chen YX, Wu HX, Yin L, Zhao Q, Luo HY, Zeng ZL, Qiu MZ and Xu RH: Integrated analysis of single-cell and bulk RNA sequencing data reveals a pan-cancer stemness signature predicting immunotherapy response. *Genome Med* 14: 45, 2022.
- Trapnell C, Cacchiarelli D, Grimsby J, Pokharel P, Li S, Morse M, Lennon NJ, Livak KJ, Mikkelsen TS and Rinn JL: The dynamics and regulators of cell fate decisions are revealed by pseudotemporal ordering of single cells. *Nat Biotechnol* 32: 381-386, 2014.
- Zheng SC, Stein-O'Brien G, Augustin JJ, Slosberg J, Carosso GA, Winer B, Shin G, Bjornsson HT, Goff LA and Hansen KD: Universal prediction of cell-cycle position using transfer learning. *Genome Biol* 23: 41, 2022.
- Liberzon A, Birger C, Thorvaldsdóttir H, Ghandi M, Mesirov JP and Tamayo P: The Molecular signatures database (MSigDB) hallmark gene set collection. *Cell Syst* 1: 417-425, 2015.
- Yu G, Wang LG, Han Y and He QY: clusterProfiler: An R package for comparing biological themes among gene clusters. *OMICS* 16: 284-287, 2012.

40. Patel AP, Tirosh I, Trombetta JJ, Shalek AK, Gillespie SM, Wakimoto H, Cahill DP, Nahed BV, Curry WT, Martuza RL, *et al*: Single-cell RNA-seq highlights intratumoral heterogeneity in primary glioblastoma. *Science* 344: 1396-1401, 2014.
41. Querec TD, Akondy RS, Lee EK, Cao W, Nakaya HI, Teuwen D, Pirani A, Gernert K, Deng J, Marzolf B, *et al*: Systems biology approach predicts immunogenicity of the yellow fever vaccine in humans. *Nat Immunol* 10: 116-125, 2009.
42. Kinoshita M, Uchida T, Sato A, Nakashima M, Nakashima H, Shono S, Habu Y, Miyazaki H, Hiroi S and Seki S: Characterization of two F4/80-positive Kupffer cell subsets by their function and phenotype in mice. *J Hepatol* 53: 903-910, 2010.
43. Zhang L, Li Z, Skrzypczynska KM, Fang Q, Zhang W, O'Brien SA, He Y, Wang L, Zhang Q, Kim A, *et al*: Single-cell analyses inform mechanisms of myeloid-targeted therapies in colon cancer. *Cell* 181: 442-459.e29, 2020.
44. Haber AL, Biton M, Rogel N, Herbst RH, Shekhar K, Smillie C, Burgin G, Delorey TM, Howitt MR, Katz Y, *et al*: A single-cell survey of the small intestinal epithelium. *Nature* 551: 333-339, 2017.
45. Qiu J, Qu X, Wang Y, Guo C, Lv B, Jiang Q, Su W, Wang L and Hua K: Single-cell landscape highlights heterogenous microenvironment, novel immune reaction patterns, potential biomarkers and unique therapeutic strategies of cervical squamous carcinoma, human papillomavirus-associated (HPVA) and non-HPVA adenocarcinoma. *Adv Sci (Weinh)* 10: e2204951, 2023.
46. van der Poel M, Ulas T, Mizze MR, Hsiao CC, Miedema SSM, Adelia, Schuurman KG, Helder B, Tas SW, Schultze JL, *et al*: Transcriptional profiling of human microglia reveals grey-white matter heterogeneity and multiple sclerosis-associated changes. *Nat Commun* 10: 1139, 2019.
47. Bassez A, Vos H, Van Dyck L, Floris G, Arijs I, Desmedt C, Boeckx B, Vanden Bempt M, Nevelsteen I, Lambein K, *et al*: A single-cell map of intratumoral changes during anti-PD1 treatment of patients with breast cancer. *Nat Med* 27: 820-832, 2021.
48. Wendisch D, Dietrich O, Mari T, von Stillfried S, Ibarra IL, Mittermaier M, Mache C, Chua RL, Knoll R, Timm S, *et al*: SARS-CoV-2 infection triggers profibrotic macrophage responses and lung fibrosis. *Cell* 184: 6243-6261.e27, 2021.
49. Gong Z, Li Q, Shi J, Li P, Hua L, Shultz LD and Ren G: Immunosuppressive reprogramming of neutrophils by lung mesenchymal cells promotes breast cancer metastasis. *Sci Immunol* 8: eadd5204, 2023.
50. Kennedy A, Waters E, Rowshanravan B, Hinze C, Williams C, Janman D, Fox TA, Booth C, Pesenacker AM, Halliday N, *et al*: Differences in CD80 and CD86 transendocytosis reveal CD86 as a key target for CTLA-4 immune regulation. *Nat Immunol* 23: 1365-1378, 2022.
51. Amiry-Moghaddam M: AQP4 and the fate of gliomas. *Cancer Res* 79: 2810-2811, 2019.
52. Hu H, Mu Q, Bao Z, Chen Y, Liu Y, Chen J, Wang K, Wang Z, Nam Y, Jiang B, *et al*: Mutational landscape of secondary glioblastoma guides MET-targeted trial in brain tumor. *Cell* 175: 1665-1678.e18, 2018.
53. Kakogiannos N, Ferrari L, Giampietro C, Scalise AA, Maderna C, Ravà M, Taddei A, Lampugnani MG, Pisati F, Malinverno M, *et al*: JAM-A acts via C/EBP- α to promote claudin-5 expression and enhance endothelial barrier function. *Circ Res* 127: 1056-1073, 2020.
54. Hosmann A, Jaber M, Roetzer-Pejrimovsky T, Timelthaler G, Borkovec M, Kiesel B, Wadiura LI, Millesi M, Mercea PA, Phillips J, *et al*: CD34 microvasculature in low-grade glioma: Correlation with 5-aminolevulinic acid fluorescence and patient prognosis in a multicenter study at three specialized centers. *J Neurosurg* 138: 1281-1290, 2023.
55. Agostini M, Amato F, Vieri ML, Greco G, Tonazzini I, Baroncelli L, Caleo M, Vannini E, Santi M, Signore G and Cecchini M: Glial-fibrillary-acidic-protein (GFAP) biomarker detection in serum-matrix: Functionalization strategies and detection by an ultra-high-frequency surface-acoustic-wave (UHF-SAW) lab-on-chip. *Biosens Bioelectron* 172: 112774, 2021.
56. Gai QJ, Fu Z, He J, Mao M, Yao XX, Qin Y, Lan X, Zhang L, Miao JY, Wang YX, *et al*: EPHA2 mediates PDGFA activity and functions together with PDGFRA as prognostic marker and therapeutic target in glioblastoma. *Signal Transduct Target Ther* 7: 33, 2022.
57. Suvà ML, Rheinbay E, Gillespie SM, Patel AP, Wakimoto H, Rabkin SD, Riggi N, Chi AS, Cahill DP, Nahed BV, *et al*: Reconstructing and reprogramming the tumor-propagating potential of glioblastoma stem-like cells. *Cell* 157: 580-594, 2014.
58. Yang Y, Chu L, Zeng Z, Xu S, Yang H, Zhang X, Jia J, Long N, Hu Y and Liu J: Four specific biomarkers associated with the progression of glioblastoma multiforme in older adults identified using weighted gene co-expression network analysis. *Bioengineered* 12: 6643-6654, 2021.
59. Bendris N, Loukil A, Cheung C, Arsic N, Rebouissou C, Hipskind R, Peter M, Lemmers B and Blanchard JM: Cyclin A2: A genuine cell cycle regulator? *Biomol Concepts* 3: 535-543, 2012.
60. Loukil A, Cheung CT, Bendris N, Lemmers B, Peter M and Blanchard JM: Cyclin A2: At the crossroads of cell cycle and cell invasion. *World J Biol Chem* 6: 346-350, 2015.
61. Liang W, Guan H, He X, Ke W, Xu L, Liu L, Xiao H and Li Y: Down-regulation of SOSTDC1 promotes thyroid cancer cell proliferation via regulating cyclin A2 and cyclin E2. *Oncotarget* 6: 31780-31791, 2015.
62. Andersen JS, Wilkinson CJ, Mayor T, Mortensen P, Nigg EA and Mann M: Proteomic characterization of the human centrosome by protein correlation profiling. *Nature* 426: 570-574, 2003.
63. O'regan L, Blot J and Fry AM: Mitotic regulation by NIMA-related kinases. *Cell Div* 2: 25, 2007.
64. Huang X, Zhang G, Tang T, Gao X and Liang T: One shoot, three birds: Targeting NEK2 orchestrates chemoradiotherapy, targeted therapy, and immunotherapy in cancer treatment. *Biochim Biophys Acta Rev Cancer* 1877: 188696, 2022.
65. Alcantara Llaguno S, Chen J, Kwon CH, Jackson EL, Li Y, Burns DK, Alvarez-Buylla A and Parada LF: Malignant astrocytomas originate from neural stem/progenitor cells in a somatic tumor suppressor mouse model. *Cancer Cell* 15: 45-56, 2009.
66. Liu C, Sage JC, Miller MR, Verhaak RG, Hippenmeyer S, Vogel H, Foreman O, Bronson RT, Nishiyama A, Luo L and Zong H: Mosaic analysis with double markers reveals tumor cell of origin in glioma. *Cell* 146: 209-221, 2011.
67. Hydrbring P, Malumbres M and Sicinski P: Non-canonical functions of cell cycle cyclins and cyclin-dependent kinases. *Nat Rev Mol Cell Biol* 17: 280-292, 2016.
68. Huang J, Li Q, Peng Q, Xie Y, Wang W, Pei C, Zhao Y, Liu R, Huang L, Li T, *et al*: Single-cell RNA sequencing reveals heterogeneity and differential expression of decidua tissues during the peripartum period. *Cell Prolif* 54: e12967, 2021.
69. Zhao T, Fu Y, Zhu J, Liu Y, Zhang Q, Yi Z, Chen S, Jiao Z, Xu X, Xu J, *et al*: Single-cell RNA-Seq reveals dynamic early embryonic-like programs during chemical reprogramming. *Cell Stem Cell* 23: 31-45.e7, 2018.
70. Balducci M, Chiesa S, Diletto B, D'Agostino GR, Mangiola A, Manfrida S, Mantini G, Albanese A, Fiorentino A, Frascino V, *et al*: Low-dose fractionated radiotherapy and concomitant chemotherapy in glioblastoma multiforme with poor prognosis: A feasibility study. *Neuro Oncol* 14: 79-86, 2012.
71. Kong L, Gao J, Hu J, Lu R, Yang J, Qiu X, Hu W and Lu JJ: Carbon ion radiotherapy boost in the treatment of glioblastoma: A randomized phase I/III clinical trial. *Cancer Commun (Lond)* 39: 5, 2019.
72. Kops GJ, Weaver BA and Cleveland DW: On the road to cancer: Aneuploidy and the mitotic checkpoint. *Nat Rev Cancer* 5: 773-785, 2005.
73. Nicholson JM and Cimini D: How mitotic errors contribute to karyotypic diversity in cancer. *Adv Cancer Res* 112: 43-75, 2011.
74. Fry AM, O'Regan L, Sabir SR and Bayliss R: Cell cycle regulation by the NEK family of protein kinases. *J Cell Sci* 125: 4423-4433, 2012.
75. Fry AM, Meraldi P and Nigg EA: A centrosomal function for the human Nek2 protein kinase, a member of the NIMA family of cell cycle regulators. *EMBO J* 17: 470-481, 1998.
76. Li JJ and Li SA: Mitotic kinases: the key to duplication, segregation, and cytokinesis errors, chromosomal instability, and oncogenesis. *Pharmacol Ther* 111: 974-984, 2006.
77. Helps NR, Luo X, Barker HM and Cohen PT: NIMA-related kinase 2 (Nek2), a cell-cycle-regulated protein kinase localized to centrosomes, is complexed to protein phosphatase 1. *Biochem J* 349: 509-518, 2000.
78. Chotiner JY, Wolgemuth DJ and Wang PJ: Functions of cyclins and CDKs in mammalian gametogenesis†. *Biol Reprod* 101: 591-601, 2019.
79. Jiang F, Luo F, Zeng N, Mao Y, Tang X, Wang J, Hu Y and Wu C: Characterization of fatty acid metabolism-related genes landscape for predicting prognosis and aiding immunotherapy in glioma patients. *Front Immunol* 13: 902143, 2022.

80. Ostrom QT, Bauchet L, Davis FG, Deltour I, Fisher JL, Langer CE, Pekmezci M, Schwartzbaum JA, Turner MC, Walsh KM, *et al.*: The epidemiology of glioma in adults: A 'state of the science' review. *Neuro Oncol* 16: 896-913, 2014.
81. Sturm D, Pfister SM and Jones DTW: Pediatric gliomas: Current concepts on diagnosis, biology, and clinical management. *J Clin Oncol* 35: 2370-2377, 2017.
82. Ashby LS and Ryken TC: Management of malignant glioma: Steady progress with multimodal approaches. *Neurosurg Focus* 20: E3, 2006.
83. Andersen BM, Faust Akl C, Wheeler MA, Chiocca EA, Reardon DA and Quintana FJ: Glial and myeloid heterogeneity in the brain tumour microenvironment. *Nat Rev Cancer* 21: 786-802, 2021.
84. Martínez-Cerdeño V and Noctor SC: Neural progenitor cell terminology. *Front Neuroanat* 12: 104, 2018.
85. Zhu Y, Guignard F, Zhao D, Liu L, Burns DK, Mason RP, Messing A and Parada LF: Early inactivation of p53 tumor suppressor gene cooperating with NF1 loss induces malignant astrocytoma. *Cancer Cell* 8: 119-130, 2005.
86. Zarco N, Norton E, Quiñones-Hinojosa A and Guerrero-Cázares H: Overlapping migratory mechanisms between neural progenitor cells and brain tumor stem cells. *Cell Mol Life Sci* 76: 3553-3570, 2019.
87. Zheng H, Ying H, Yan H, Kimmelman AC, Hiller DJ, Chen AJ, Perry SR, Tonon G, Chu GC, Ding Z, *et al.*: p53 and Pten control neural and glioma stem/progenitor cell renewal and differentiation. *Nature* 455: 1129-1133, 2008.
88. Jung E, Alfonso J, Osswald M, Monyer H, Wick W and Winkler F: Emerging intersections between neuroscience and glioma biology. *Nat Neurosci* 22: 1951-1960, 2019.
89. Schonberg DL, Lubelski D, Miller TE and Rich JN: Brain tumor stem cells: Molecular characteristics and their impact on therapy. *Mol Aspects Med* 39: 82-101, 2014.
90. Kohwi M and Doe CQ: Temporal fate specification and neural progenitor competence during development. *Nat Rev Neurosci* 14: 823-838, 2013.
91. Yabo YA, Niclou SP and Golebiewska A: Cancer cell heterogeneity and plasticity: A paradigm shift in glioblastoma. *Neuro Oncol* 24: 669-682, 2022.
92. Lathia JD, Mack SC, Mulkearns-Hubert EE, Valentim CL and Rich JN: Cancer stem cells in glioblastoma. *Genes Dev* 29: 1203-1217, 2015.
93. Liu L, Michowski W, Kolodziejczyk A and Sicinski P: The cell cycle in stem cell proliferation, pluripotency and differentiation. *Nat Cell Biol* 21: 1060-1067, 2019.
94. Meacham CE and Morrison SJ: Tumour heterogeneity and cancer cell plasticity. *Nature* 501: 328-337, 2013.
95. Roninson IB, Broude EV and Chang BD: If not apoptosis, then what? Treatment-induced senescence and mitotic catastrophe in tumor cells. *Drug Resist Updat* 4: 303-313, 2001.
96. Castro-Gamero AM, Pezuk JA, Brassesco MS and Tone LG: G2/M inhibitors as pharmacotherapeutic opportunities for glioblastoma: The old, the new, and the future. *Cancer Biol Med* 15: 354-374, 2018.



Copyright © 2024 Zhou et al. This work is licensed under a Creative Commons Attribution-NonCommercial-NoDerivatives 4.0 International (CC BY-NC-ND 4.0) License.